

Article

Structure Robustness of Highly Dispersed Pt/Al₂O₃ Catalyst for Propane Dehydrogenation during Oxychlorination Regeneration Process

Lu Dong ¹, Yitong Sun ¹, Yifan Zhou ¹, Zhijun Sui ^{1,*} , Yunsheng Dai ^{2,*}, Yian Zhu ¹ and Xinggui Zhou ¹ 

- ¹ State Key Laboratory of Chemical Engineering, East China University of Science and Technology, 130 Meilong Road, Shanghai 200237, China; donglu2023@sina.com (L.D.); syt20170601@163.com (Y.S.); zyf_ecust@163.com (Y.Z.); yanzhu@ecust.edu.cn (Y.Z.); xgzhou@ecust.edu.cn (X.Z.)
- ² State Key Laboratory of Advanced Technologies for Comprehensive Utilization of Platinum Metals, Sino-Platinum Metals Co., Ltd., Kunming Institute of Precious Metals, Kunming 650106, China
- * Correspondence: zhjsui@ecust.edu.cn (Z.S.); daiysh@ipm.com.cn (Y.D.)

Abstract: The structure and performance stability of a Pt-based catalyst for propane dehydrogenation during its reaction–regeneration cycles is one of the key factors for its commercial application. A 0.3% Pt/Al₂O₃ catalyst with a sub-nanometric particle size was prepared and two different types of regeneration processes, long-term dichloroethane oxychlorination and a reaction–oxidation–oxychlorination cycle, were investigated on this catalyst. The fresh, sintered and regenerated catalyst was characterized by HAADF-STEM, CO-DRIFTS, XPS, CO chemisorption and N₂ physisorption, and its catalytic performance for propane dehydrogenation was also tested. The results show that the catalysts tend to have a similar particle size, coordination environment and catalytic performance with the extension of the regeneration time or an increase in the number of cycles in the two regeneration processes, and a common steady state could be achieved on the catalysts. This indicates that structure of the catalyst tends to approach its equilibrium state in the regeneration process, during which the utilization efficiency of Pt is maximized by increasing the dispersion of Pt and its intrinsic activity, and the structural robustness is secured. The performance of the catalyst is comparable to that of a single-atom Pt/Al₂O₃ catalyst.

Keywords: propane dehydrogenation; supported Pt catalyst; regeneration; oxychlorination; re-dispersion; sintering



Citation: Dong, L.; Sun, Y.; Zhou, Y.; Sui, Z.; Dai, Y.; Zhu, Y.; Zhou, X. Structure Robustness of Highly Dispersed Pt/Al₂O₃ Catalyst for Propane Dehydrogenation during Oxychlorination Regeneration Process. *Catalysts* **2024**, *14*, 48. <https://doi.org/10.3390/catal14010048>

Academic Editors: Bin Xu and Yu Gong

Received: 12 December 2023

Revised: 30 December 2023

Accepted: 8 January 2024

Published: 10 January 2024



Copyright: © 2024 by the authors. Licensee MDPI, Basel, Switzerland. This article is an open access article distributed under the terms and conditions of the Creative Commons Attribution (CC BY) license (<https://creativecommons.org/licenses/by/4.0/>).

1. Introduction

Propane dehydrogenation (PDH) is the preferred method for on-purpose propylene production, in which a supported Pt-based catalyst is widely used [1]. However, these Pt-based PDH catalysts still suffer from coking problems and require frequent regeneration to restore their catalytic performance [2,3]. In the regeneration process, the catalyst is firstly oxidized under a high temperature in an oxidation atmosphere to remove the accumulated cokes, during which the Pt sintering problem occurs [4,5]. Then, the re-dispersion of Pt through oxychlorination treatment using Cl₂ or HCl as the chlorine source is carried out to fully recover the catalyst's performance [2,6]. Therefore, the oxychlorination process has a great influence on the catalyst's stability and the economics of the process.

For the oxychlorination of a Pt-based propane/butane catalyst, very few studies have been reported [4,7–10] and this topic is not included in the recent reviews. A concise summary of the oxychlorination of Pt-based catalytic reforming catalysts can be found in the literature [7]. Choi et al. [7] introduced hydrochloric acid into a Pt-Sn/Al₂O₃ PDH catalyst after coke burning and found that oxychlorination-like conditions could be formed during calcination in the air, leading to the regeneration of the catalyst. The effectiveness of regenerating a series Pt-Sn/Al₂O₃ PDH catalyst by dichloroethane oxychlorination

has also been verified, and the performance of the regenerated catalyst was found to be a function of the oxychlorination conditions, which suggests that the coordination environment of Pt should be considered to optimize the catalyst [9]. Anstice et al. [10] used 1,2-dichloropropane as a chlorinating agent to regenerate a γ -Al₂O₃ supported 3 wt% Pt–4.5 wt% Sn catalyst for a butane/H₂ reaction. The results suggested that the addition of 1,2-dichloropropane before the reduction of the catalyst could induce the formation of the Pt₁Sn₁ alloy and increase the dehydrogenation selectivity. Masoudian et al. [8] investigated the regeneration of a commercial Pt–Sn/ γ -Al₂O₃ catalyst for isobutane dehydrogenation using HCl and Cl₂ as oxychlorination agents. The dispersion of the regenerated catalyst was close to that of the fresh catalyst, as was its catalytic activity.

Recently, some highly dispersed (single-atom, cluster or subnanosized) Pt catalysts with enhanced metal–support interactions were reported to be effective PDH catalysts, showing low deactivation rates and good structural stability [11–17]. However, it should be noted that these catalysts are usually tested under a reaction temperature below 600 °C, which is lower than the industrial PDH reactor inlet temperature. This means that the coking problem may be underestimated [18] and, as a consequence, so is the sintering problem during coking oxidation due to the exothermic effect of this reaction. The necessity of the re-dispersion of these highly dispersed catalysts by oxychlorination treatment needs to be further verified, especially for those with the absence of promoters, to enhance metal dispersion, e.g., Sn, etc.

The oxychlorination of supported metal catalysts involves complex physical and chemical processes, such as metal species transformation, the detachment of metal atoms from large particles, the migration and anchoring of metal species on the carrier surface and metal aggregation [19–22]. From a kinetic point of view, the re-dispersion process can be seen as the reversible process of microcrystalline growth, and the tendency to sinter or and disperse in metals is related to the operating conditions [23–25]. When the equilibrium of the process is reached, a limit of metal dispersion could be obtained under specified treatment conditions for a given catalyst, which is the driving force of the re-dispersion kinetics and affects the structural stability of the regenerated catalyst [24,26–29]. From a thermodynamic point of view, the particle size of Pt in the equilibrium state is a function of the metal/support adhesion energy, the surface energy of Pt and the metal's bulk sublimation enthalpy [23,30], which measures the Pt–support, surface Pt–Pt/adatoms and bulk Pt–Pt interaction, respectively. When the supported metal particle size decreases to the sub-nanoscale, the metal–support adhesion energy and metal surface energy increase [31] and then the equilibrium as well the dispersion kinetics of these catalysts may differ from those of nanosized supported catalysts. Unfortunately, re-dispersion research in the early years was usually carried out on catalysts with a particle size of several to tens of nanometers. The re-dispersion behavior of highly dispersed catalysts by oxychlorination and its influence on the catalyst structure and catalytic performance needs to be further addressed.

In this work, long-term oxychlorination treatment and multiple cycles of reaction–oxidation–oxychlorination treatment of a highly dispersed Pt/Al₂O₃ catalyst were adopted to examine whether the catalyst could approach to an equilibrium state, and then to verify the effectiveness of the re-dispersion of the sintered supported Pt catalyst to regain its sub-nanometer size without the help of a Sn promoter. The evolution of the structural properties, e.g., particle size, electronic structure and coordination environment, etc., and the PDH performance of Pt during the oxychlorination treatment were explored. These results could be valuable for the development of high-performance Pt-based PDH catalysts with high structural stability during repeated reaction–regeneration cycles and pave the way for the application of highly dispersed supported metal catalysts by addressing the concern regarding their structural robustness.

2. Results

2.1. Characterization

The XRD results in Figure 1a show that all the catalyst samples exhibit obvious diffraction peaks at 31° , 32° , 37° , 40° , 45° and 67° , which are similar to those of typical $\theta\text{-Al}_2\text{O}_3$ (PDF NO#35-0121). No obvious Pt diffraction peak can be observed in any of the samples, indicating that Pt is highly dispersed or exists in an amorphous state. Figure 1b shows the nitrogen adsorption isotherms of the catalyst. It can be seen that all the samples have type IV adsorption isotherms, with obvious H3-type hysteresis loops, indicating that the pores are mesoporous and macroporous, with irregular shapes [32]. The specific surface area, average pore size and total pore volume of the catalysts are listed in Table 1, and the curves of the pore size distribution are shown in Figure 1c. It is obvious that, except for the fresh catalysts, all catalysts have very similar textural properties and pore structures. The slight difference in the fresh sample compared to the others may be due to the lower calcination temperature used for the catalyst's preparation. Figure 1d shows the SEM image of the fresh sample, which shows that the morphology of the sample is irregular and the chunks are composed of particles with different sizes adhering to each other. After sintering or regenerating fresh catalysts, the morphological characteristics remain unchanged (the images are not shown here). These results testify that, after sintering and two types of regeneration treatment, the samples have a similar crystal phase, morphology and textural properties, and changes in these properties have a minor effect on the supported catalysts.

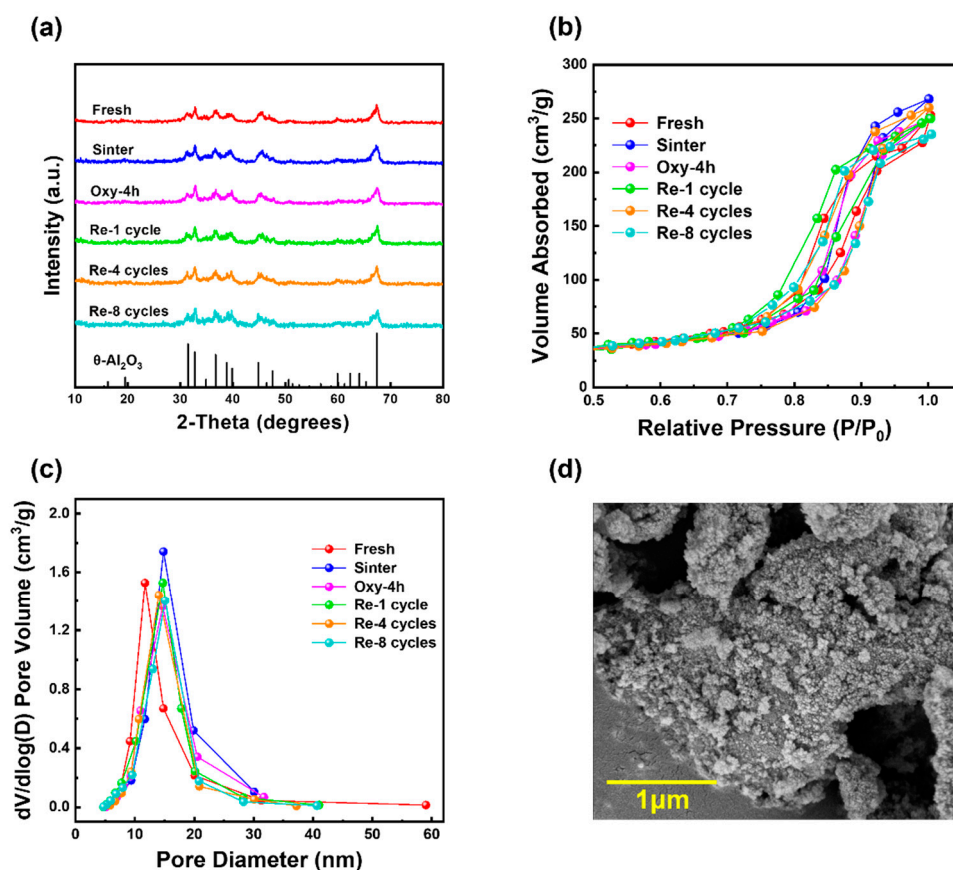


Figure 1. The characterization results of different samples: (a) XRD, (b) N_2 physisorption isotherms, (c) pore diameter distribution and (d) SEM images.

Figure 2 shows the HAADF-STEM images of different samples. It can be found that Pt is evenly distributed on the carrier. The average particle size of Pt in the fresh catalyst is 0.91 nm and increases to 1.20 nm after sintering (as shown in Figure 2a,b). When gradually extending the oxychlorination time, the Pt particle size decreases and approaches 0.95 nm

after 4 hours of treatment (Figure 2e). After one, four and eight cycles of oxychlorination, the average particle sizes of Pt are 1.04 nm, 0.95 nm and 0.93 nm, respectively. The amplitude of the change in particle size gradually decreases and finally approaches a quasi-stable state. The Oxy-4 h and Re-8 cycle samples have a similar particle size, indicating that, despite the differences in the two regeneration processes, the Pt particles could achieve similar dispersion.

Table 1. Textural and structural properties and catalytic performance of different samples.

Sample	S _{BET} ¹ (m ² /g)	D _{pore} ¹ (nm)	V _{pore} ¹ (cm ³ /g)	Pt Dispersion ² (%)	Pt ⁴⁺ Ratio ³ (%)	TOF (s ⁻¹)
Fresh	88.1	12.5	0.35	80.2	24.1	1.96
Sintered	78.9	14.8	0.36	48.3	35.3	1.58
Oxy-30 min	82.3	13.4	0.37	60.5	27.0	1.84
Oxy-1 h	85.1	14.0	0.36	70.8	23.3	1.88
Oxy-4 h	81.7	13.8	0.33	73.5	22.0	1.86
Re-1 cycle	87.5	14.3	0.39	59.5	28.0	1.42
Re-4 cycles	84.8	14.0	0.37	69.4	26.9	1.48
Re-8 cycles	83.4	14.2	0.39	72.4	21.1	1.84

¹ Determined from N₂ physisorption, ² determined from CO chemisorption, ³ determined from XPS.

The dispersion of Pt in the catalyst determined from CO chemisorption characterization is shown in Table 1. The gradual increase in dispersion can be observed, consistent with the results obtained from HAADF-STEM, although the calculated average particle sizes are slightly different from those determined by the HAADF-STEM characterizations. The difference in the results obtained from these two methods has also been reported previously [9,33], and it may be caused by the unique morphology and/or local coordination environment of the Pt [22,34]. The close dispersion of the Oxy-4 h and Re-8 cycles confirms that a similar dispersion limit of Pt could be reached after both the regeneration processes.

The CO-DRIFTS characterization results are shown in Figure 3. The absorption peak around 2000–2100 cm⁻¹ can be found on all the samples, which is caused by CO linear adsorption on Pt with different coordination numbers [28,35–37]. The ~1820 cm⁻¹ absorption peak, attributed to the bridge adsorption of CO on Pt–Pt multiple sites [36], can be observed on the fresh and sintered samples, which indicates that some aggregated Pt atoms exist on these two samples, even though the fresh sample has a smaller particle size, determined by the HAADF STEM results, than the Oxy-4 h and Re-8 cycle samples. This peak can also be found on the Re-1 cycle sample, but not on Oxy-30 min, which underwent a similar oxychlorination treatment. The temperature of the precedent oxidation process for these two samples was identical, but some cokes accumulated on the Re-1 cycle sample before its oxidation, and the actual oxidation temperature on the sample surface should be higher due to the exothermic coke oxidation reaction, which will lead to the more severe sintering of Pt [38]. With the extension of the Oxy process time or an increase in the number of recycle processes, a more even distribution of Pt is achieved, as evidenced by the disappearance of the peak around 1820 cm⁻¹. The spectra of the Oxy-4 h and Re-8 cycles are very similar according to the peak temperature and peak area ratio between different adsorption peaks, which indicates that the distribution of Pt and the local coordination environment of Pt in these two samples tend to approach a similar stable state.

The XPS characterization results are shown in Figure 4. The Pt 4d orbital signal is used to characterize the electronic valence state of Pt due to the partial overlap between the Pt 4f and Al 2p orbitals. The characteristic peaks in the regions of 316.8–318.5 eV, 314.6–315.6 eV and 311.8–312.9 eV can be attributed to Pt⁴⁺, Pt²⁺ and Pt⁰, respectively [4,39]. The higher content of Pt⁴⁺ in the sintered catalyst is consistent with the research results of Le Normand et al. [29] and indicated that the surface of Pt is covered with PtO₂. The content of Pt⁴⁺ significantly decreases after regeneration, which suggests that the Cl introduced in the oxychlorination process interacts with Pt, and Pt-O-Cl species are formed to facilitate the

migration and dispersion of Pt in the sintered catalyst [21,22,26,40]. As the regeneration proceeds in both the Oxy process and recycle process, the peak area ascribed to Pt⁴⁺ decreases and finally achieves a quasi-steady state, reaching 22.0% and 21.1% of the total peak area in the Re-8 cycle and Oxy-4 h samples, respectively. These results indicate that the electronic structure of Pt tends to show some common features, although the samples underwent different regeneration processes.

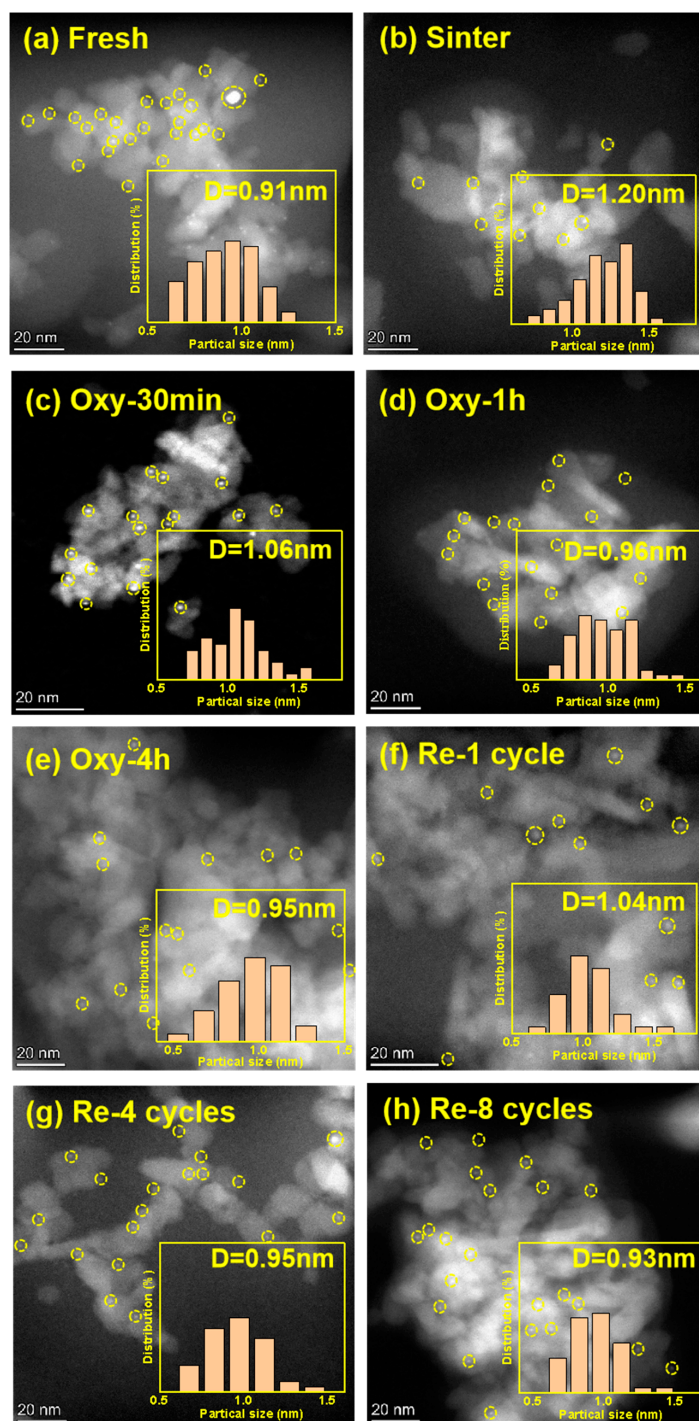


Figure 2. HAADF-STEM images of different samples: (a) fresh, (b) sintered, (c) Oxy-30 min, (d) Oxy-1 h, (e) Oxy-4 h, (f) Re-1 cycle, (g) Re-4 cycles, (h) Re-8 cycles. The dotted circles indicate the presence of Pt particles.

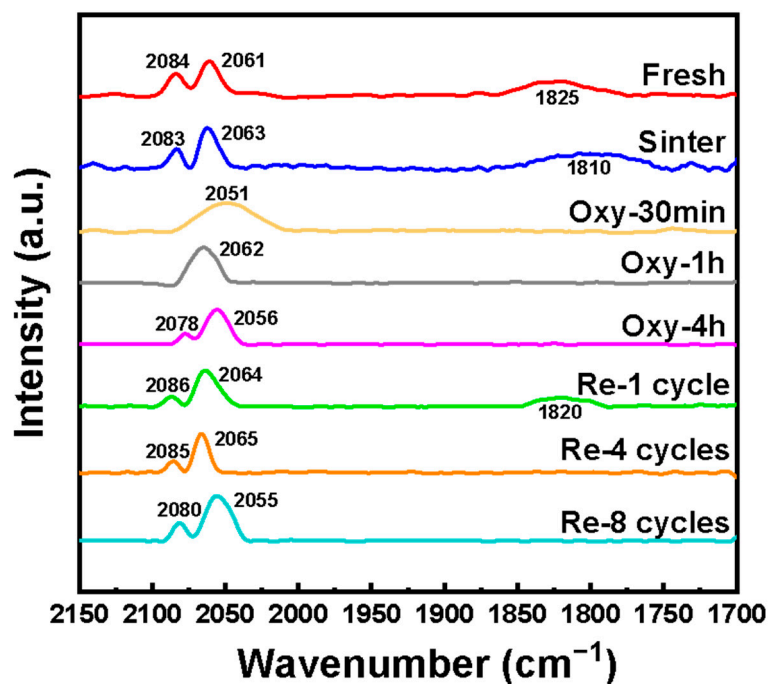


Figure 3. CO-DRIFTS spectra of different samples.

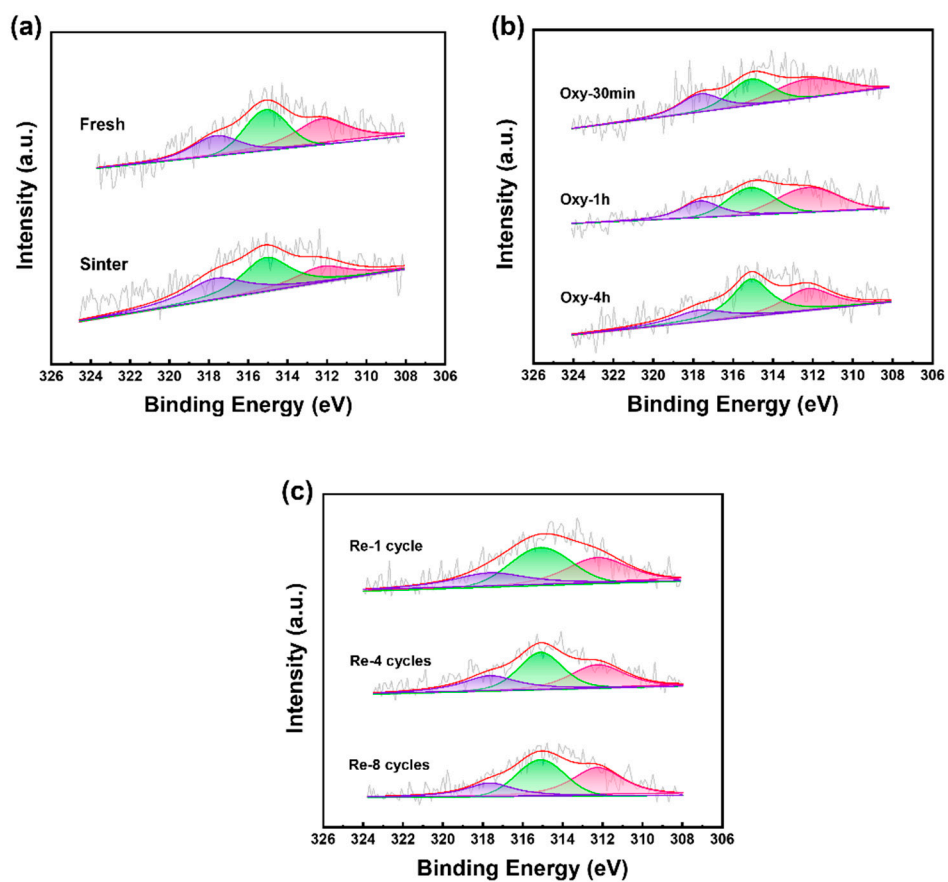


Figure 4. XPS spectra of different samples. The colored area indicates the peak deconvolution results: purple, Pt^{4+} ; green, Pt^{2+} ; pink, Pt^0 and red, summation of the three peaks. (a) Fresh and Sinter catalyst, (b) catalysts after Oxy process, (c) catalysts after Recycle process.

2.2. Catalytic Performance

Figure 5 shows the results of the catalytic performance test. The initial conversion of the fresh catalyst was 21.7%, which decreased to 9.9% after sintering. With the increase in the number of cycles in the regeneration process, the PDH activity of the catalyst gradually increased from 10.9% to 13.2% and tended to stabilize at 17.1% after eight cycles, which is close to the 17.6% conversion obtained on Oxy-4 h. The selectivity over all the catalysts is higher than 92% at the initial stage of the reaction and tends to increase and stabilize in the range of ~92–96%, which is close to that obtained on an alumina-supported single-atom Pt catalyst [41], indicating that the Pt is highly dispersed. The Oxy-4 h and Re-8 cycles have the same selectivity of ~95.0%, apparently higher than those on fresh, sintered and other samples. The coke amounts determined by TG in these two samples are also close, at 2.17 wt% and 2.14 wt%, respectively. The similarity of the catalytic performance over these two catalysts can be seen as a consequence of their similar structural properties, as these results are sensitive to the catalyst's structural properties and can be used for reactive characterization [42].

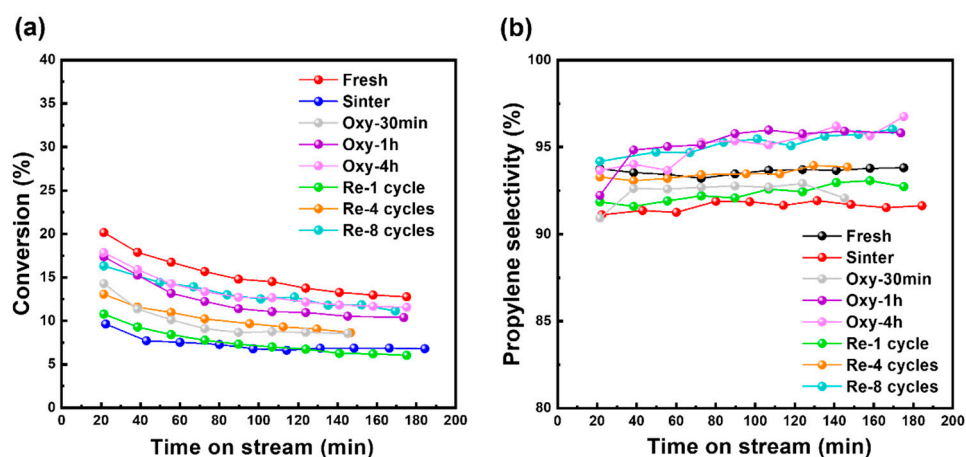


Figure 5. Catalytic performance of different samples: (a) propane conversion and (b) propylene selectivity.

3. Discussion

The similarity in the structure and performance of the Oxy-4 h and Re-8 cycle samples demonstrates that the highly dispersed Pt/Al₂O₃ catalysts tend to approach a quasi-equilibrium state. This state corresponds to the ‘maximum allowable catalyst dispersion’ of Pt/Al₂O₃ with a Pt particle size of several nanometers during the HCl oxychlorination re-dispersion process [24], or the ‘equilibrium radius’ of nanosized metal particles during the sintering process [43], which is the source of the driving force for the reversible sintering/re-dispersion kinetics. This thermodynamic equilibrium state indicates that the structure of the highly dispersed Pt catalyst for PDH could be fully restored if the catalyst is properly regenerated and is robust during the reaction–regeneration cycles, although the sintering of Pt could occur during oxidation in the coke process.

The gradual approach of the quasi-equilibrium state during the re-dispersion of the supported Pt catalyst can also be used to boost its catalytic performance. After the re-dispersion process, more Pt atoms could be exposed to the reaction atmosphere due to the increase in metal dispersion. Moreover, the TOF for propane conversion (see Table 1) also increases, which is calculated according to the following formula:

$$\text{TOF} = \frac{C_3H_8, \text{conversion}}{m_{\text{cat}}} \times \frac{F_{C_3H_8}}{W_{t_{\text{Pt loading}}} \times \frac{D_{\text{Pt}}}{M_{\text{Pt}}}} \quad (1)$$

where $C_3H_8, \text{conversion}$ and $F_{C_3H_8}$ are the initial propane conversion (%) and inlet propane flow rate (mol/s), respectively; m_{cat} , $W_{t_{\text{Pt loading}}}$, D_{Pt} and M_{Pt} are the catalyst loading amount (g), Pt loading on the catalyst (wt%), Pt dispersion (%) and molecular weight of Pt (g/mol).

These results verify that the utilization efficiency of Pt could be maximized during the re-dispersion process. Meanwhile, the selectivity to propene increases and the coking reaction decreases due to the isolation of Pt atoms and diminishment of multi-Pt–Pt bonds to catalyze the side reaction of PDH [44,45].

In the process of catalyst regeneration, the change in the particle size indicates that Pt atoms can detach from large particles and migrate on the surface of the carrier, be gradually anchored at different sites of alumina and, finally, reach a quasi-steady state after long-term regeneration. The DFT results obtained by Zhou et al. [46] demonstrate that the oxychlorination reaction can reduce the minimum temperature of Pt evaporation and increase the maximum allowable temperature of the capture of Pt species, which leads to a thermodynamically favored re-dispersion process. Further, Li et al. [47] show the universal volcano dependence of the metal nanoparticle's sintering kinetics on the metal–support binding energy, which can be used as a single descriptor to predict nanoparticle growth rates. A strong Pt–support interaction would be helpful for the dispersion of Pt, and Pt tends to be anchored, during its migration on the support surface, on sites with strong interaction, enhancing its structural stability [48,49]. The catalytic performance could also benefit from the changing of the anchoring sites of Pt and metal–support interaction, as verified by the above, as well as others', experimental results [34,50,51] and DFT calculation results [52,53]. Furthermore, the tendency for Pt anchoring on sites with strong metal–support interaction during the oxychlorination process would ensure the structural robustness of the catalyst during reaction–regeneration cycles, although sintering may occur during the coke oxidation process.

The steady state of the catalyst after regeneration is influenced by several factors, e.g., the loading of Pt, carrier properties and oxychlorination treatment conditions [54–57]. From a catalyst development point of view, special attention should be paid to the carrier surface properties because these properties are key to determine the performance and structural stability of the Pt-based catalyst for PDH [15]. Due to the unavoidable coking problem, the catalyst regeneration process is still needed for Pt-based PDH catalysts to recover their performance. During repeated reaction–regeneration cycles, it is reasonable to conclude that the catalyst structure tends to approach its equilibrium state, as shown in this study. Then, the anchoring site for Pt and its local coordination environment are largely determined by the carrier surface properties and Pt–support interaction. Given a certain amount of Pt loading, tailoring suitable carrier surface properties can help Pt to selectively reside on these sites with a strong Pt–support interaction and retain its structural robustness and performance stability throughout its whole usage lifetime.

The influence of the oxychlorination conditions on the steady state of the regenerated catalyst can be interpreted from a dispersion kinetics point of view. In a dichloroethane oxychlorination process, the dichloroethane is dissociated in the oxidation atmosphere to generate active chlorine species through various mechanisms [22]. Therefore, the reactant concentration and temperature would influence the formation rate of the key species for re-dispersion, Pt–O–Cl and the mobility of these complexes. The re-dispersion efficiency is determined by the competitiveness between the sintering and dispersion rate. For example, increasing the temperature promotes chlorine dissociation and may enhance re-dispersion. However, it also decreases the metal–support interaction, increases the mobility of metal species and may increase the sintering rate [22]. As a result, the final steady catalyst structure may be a function of the oxychlorination conditions, and further study of the detailed re-dispersion kinetics would be helpful for the application of highly dispersed catalysts in PDH. Lastly, the calcination temperature also affects the re-dispersion efficiency. On one hand, metal particles are mobile during the process, leading a change in the metal structure; on the other hand, the surface and structural properties of the alumina support may also be altered. The influence of this factor needs to be further addressed.

4. Materials and Methods

The incipient wetness impregnation method was adopted to prepare the fresh Pt/Al₂O₃ catalyst using H₂PtCl₆·6H₂O aqueous solution as the precursor and θ-Al₂O₃ obtained from calcining a boehmite (PURALOX, Sasol Ltd., Oklahoma, OK, USA) at 1000 °C for 6 h as the carrier. The precursor solution was adjusted to obtain different Pt loadings and added to the carrier dropwise with continuous stirring. The impregnated sample was aged at room temperature for 12 h, dried in a 120 °C oven for 8 h and then placed in a muffle furnace to be heated to 500 °C at 10 °C/min, where it remained for 3 h to obtain the fresh catalyst (referred to as fresh hereafter). The sintered catalyst (referred to as sintered hereafter) was prepared by heating the fresh catalyst in a muffle furnace at a ramp of 10 °C/min to 650 °C, where it remained for 4 h.

Two types of oxychlorination regeneration processes were adopted here. The first one (Oxy process) was the regeneration of the catalysts under fixed conditions: temperature, 500 °C; oxygen concentration, 20 vol%; dichloroethane flow rate, 351 μmol/min; and various treatment durations. Ar was used as a balance gas to maintain a total flow rate of 80 mL/min. In each experiment, 0.1 g sample was loaded in the reactor. The obtained sample was called Oxy-* (* refers to different treatment times). The second one (recycle process) was a cycling process: the sintered catalyst was firstly tested for its catalytic performance under the following conditions: catalyst loading, 0.1 g; reaction temperature, 575 °C; inlet flow rate of hydrogen, propane and argon, 16, 12.8 and 47.2 mL/min, respectively; and reaction duration, 3 h. Then, an oxidation process (temperature, 500 °C; air atmosphere; treatment time, 1 h) was carried out to remove the accumulated cokes, and finally the oxychlorination treatment under the same conditions as Oxy-30 min was run. The recycle process was carried out for different times and the samples after 1, 4 and 8 cycles were denoted as Re-1 cycles, Re-4 cycles and Re-8 cycles, respectively.

An ASAP2020 instrument (Micromeritics Instrument Corporation, Norcross, GA, USA) was used to carry out the nitrogen physical adsorption to obtain information on the specific surface area, pore volume and pore size distribution of the catalysts. The samples were degassed under a vacuum at 300 °C for 4 h before the measurement, which was carried out under −196 °C. Carbon monoxide chemisorption (CO Chem) was carried out on the AutoChem2920 chemisorption instrument (Micromeritics Instrument Corporation, Norcross, GA, USA) to obtain the dispersion of Pt. The sample was firstly reduced in 10 vol% H₂/Ar at 300 °C for 1 h and then cooled down to 30 in Ar. Afterwards, the CO pulse was injected repeatedly until the saturation adsorption of the sample was reached. X-ray diffraction (XRD) was performed on a D & advantage X-ray diffractometer (Cu Kα radiation, λ = 1.5406 Å, Bruker Corporation, Billerica, MA, USA) operated at 40 kV and 30 mA to characterize the crystal structure of the catalyst. The scanning speed was 5°/min and the scanning angle was 10–80°. Field emission scanning electron microscopy (SEM) was used to observe the morphological characteristics of the catalyst on a S4800 field emission scanning electron microscope (Hitachi Ltd., Tokyo, Japan). The SE2 detector was used, with an acceleration voltage of 20 kV and a working distance of 6 mm. The X-ray photoelectron spectroscopy (XPS) characterization was carried out on an ESCALAB 250Xi spectrometer (Thermo Scientific, Waltham, MA, USA) to collect the full spectrum scanning information at 0–1200 eV and the scanning spectrum of Pt. The particle size and distribution of active metals were observed on a high-angle annular dark field scanning transmission electron microscope (HAADF-STEM) and a Jem-2100F electron microscope (JEOL Ltd., Musashino, Japan) operated at a 200 kV accelerating voltage. The particle size distribution of Pt was determined by the statistics of about 250 metal particles. Thermogravimetric analysis (TG) was performed using a Pyris 1 thermogravimetric analyzer (PerkinElmer Instruments Co., Ltd., Waltham, MA, USA) to characterize the coke content of the catalyst after the reaction. The catalyst was heated from room temperature to 800 °C under an air atmosphere. Carbon monoxide diffuse reflectance Fourier transform infrared (CO-DRIFTS) was used to obtain the spectra of the adsorption of CO on the metal, using a PerkinElmer Spectrum 100 FTIR spectrometer equipped with a liquid nitrogen-cooled MCT detector

(PerkinElmer Instruments Co., Ltd, Waltham, MA, USA). The sample powder (~50 mg) was reduced in pure hydrogen (20 mL/min) at 200 °C for 0.5 h and cooled down to 30 °C in Ar (20 mL/min). Then, the background spectrum of the sample was scanned under argon gas. After this, CO was introduced for 30 min and purged with argon (20 mL/min) for 1 h; the FT-IR spectra were recorded in the scanning range of 4000–400 cm⁻¹.

5. Conclusions

The regeneration of a sintered, highly dispersed Pt/Al₂O₃ catalyst by dichloroethane oxychlorination treatment was verified to recover its catalytic performance. A quasi-steady structure of the catalyst could be achieved through either long-term treatment or multiple reaction–oxidation–oxychlorination cycles, which was evidenced by the similar particle size distribution, coordination environment and electronic structure of Pt and the catalytic performance of the catalyst. The steady catalytic activity (TOF for propane conversion, ~1.9 s⁻¹) and selectivity to propene (~95%) were close to those of single-atom Pt/Al₂O₃. The strong Pt–support interaction is the key to maintaining the steady structure and, consequently, the catalytic performance of the catalyst during reaction–regeneration cycles.

Author Contributions: L.D.: investigation, writing—original draft preparation. Y.S.: investigation. Y.Z. (Yifan Zhou): investigation. Z.S.: conceptualization, methodology, writing—review and editing, funding acquisition. Y.D.: funding acquisition, writing—review and editing. Y.Z. (Yian Zhu): writing—review and editing. X.Z.: resources, supervision. All authors have read and agreed to the published version of the manuscript.

Funding: This research was funded by the Natural Science Foundation of China, grant number 22278130, and the Foundation of Yunnan Province Science and Technology Department, grant number 202305AF150194.

Data Availability Statement: The data presented in this study are available in the article.

Conflicts of Interest: Yunsheng Dai was employed by the Sino-Platinum Metals Co., Ltd. The remaining authors declare that the research was conducted in the absence of any commercial or financial relationships that could be construed as a potential conflict of interest.

References

- Otroshchenko, T.; Jiang, G.; Kondratenko, V.A.; Rodemerck, U.; Kondratenko, E.V. Current status and perspectives in oxidative, non-oxidative and CO₂-mediated dehydrogenation of propane and isobutane over metal oxide catalysts. *Chem. Soc. Rev.* **2021**, *50*, 473–527. [[CrossRef](#)]
- Sattler, J.J.H.B.; Ruiz-Martinez, J.; Santillan-Jimenez, E.; Weckhuysen, B.M. Catalytic Dehydrogenation of Light Alkanes on Metals and Metal Oxides. *Chem. Rev.* **2014**, *114*, 10613–10653. [[CrossRef](#)]
- Dai, Y.; Gao, X.; Wang, Q.; Wan, X.; Zhou, C.; Yang, Y. Recent progress in heterogeneous metal and metal oxide catalysts for direct dehydrogenation of ethane and propane. *Chem. Soc. Rev.* **2021**, *50*, 5590–5630. [[CrossRef](#)] [[PubMed](#)]
- Kim, G.H.; Jung, K.-D.; Kim, W.-I.; Um, B.-H.; Shin, C.-H.; Oh, K.; Koh, H.L. Effect of oxychlorination treatment on the regeneration of Pt-Sn/Al₂O₃ catalyst for propane dehydrogenation. *Res. Chem. Intermed.* **2016**, *42*, 351–365. [[CrossRef](#)]
- Behafarid, F.; Roldan Cuenya, B. Towards the Understanding of Sintering Phenomena at the Nanoscale: Geometric and Environmental Effects. *Top. Catal.* **2013**, *56*, 1542–1559. [[CrossRef](#)]
- Chen, S.; Chang, X.; Sun, G.; Zhang, T.; Xu, Y.; Wang, Y.; Pei, C.; Gong, J. Propane dehydrogenation: Catalyst development, new chemistry, and emerging technologies. *Chem. Soc. Rev.* **2021**, *50*, 3315–3354. [[CrossRef](#)]
- Choi, Y.S.; Oh, K.; Jung, K.-D.; Kim, W.-I.; Koh, H.L. Regeneration of Pt-Sn/Al₂O₃ Catalyst for Hydrogen Production through Propane Dehydrogenation Using Hydrochloric Acid. *Catalysts* **2020**, *10*, 898. [[CrossRef](#)]
- Masoudian, S.K.; Sadighi, S.; Abbasi, A.; Salehirad, F.; Fazlollahi, A. Regeneration of a Commercial Catalyst for the Dehydrogenation of Isobutane to Isobutene. *Chem. Eng. Technol.* **2013**, *36*, 1593–1598. [[CrossRef](#)]
- Zhao, F.-C.; Yang, H.; Sui, Z.-J.; Zhu, Y.-A.; Chen, D.; Zhou, X.-G. Self-adaptive structure and catalytic performance of the Pt-Sn/Al₂O₃ propane dehydrogenation catalyst regenerated by dichloroethane oxychlorination. *Catal. Sci. Technol.* **2022**, *12*, 7171–7181. [[CrossRef](#)]
- Anstice, P.J.C.; Becker, S.M.; Rochester, C.H. The effects of Cl-induced alloying in Pt-Sn/Al₂O₃ catalysts on butane/H₂ reactions. *Catal. Lett.* **2001**, *74*, 9–15. [[CrossRef](#)]
- Rochlitz, L.; Pessemesse, Q.; Fischer, J.W.A.; Klose, D.; Clark, A.H.; Plodinec, M.; Jeschke, G.; Payard, P.-A.; Coperet, C. A Robust and Efficient Propane Dehydrogenation Catalyst from Unexpectedly Segregated Pt₂Mn Nanoparticles. *J. Am. Chem. Soc.* **2022**, *144*, 13384–13393. [[CrossRef](#)] [[PubMed](#)]

12. Liu, X.; Wang, X.; Zhen, S.; Sun, G.; Pei, C.; Zhao, Z.-J.; Gong, J. Support stabilized PtCu single-atom alloys for propane dehydrogenation. *Chem. Sci.* **2022**, *13*, 9537–9543. [[CrossRef](#)] [[PubMed](#)]
13. Zhu, X.; Chen, B.; Wang, X. High active and stable structure of PtBi_{0.5}K₄/Si-Beta catalyzing propane dehydrogenation. *Chem. Eng. J.* **2023**, *474*, 145894. [[CrossRef](#)]
14. Zhang, B.; Wu, Z.; Xing, S.; Zhang, J.; Zhao, S.; Xiong, M.; Luo, J.; Qin, Y.; Gao, Z. Small-Molecule Modification Provides Pt Nucleation Sites for Enhanced Propane Dehydrogenation Performance. *J. Phys. Chem. C* **2023**, *127*, 5754–5762. [[CrossRef](#)]
15. Wang, G.; Yin, C.; Feng, F.; Zhang, Q.; Fu, H.; Bing, L.; Wang, F.; Han, D. Recent Progress on Catalyst Supports for Propane Dehydrogenation. *Curr. Nanosci.* **2023**, *19*, 473–483. [[CrossRef](#)]
16. Zhou, J.; Zhang, Y.; Liu, H.; Xiong, C.; Hu, P.; Wang, H.; Chen, S.; Ji, H. Enhanced performance for propane dehydrogenation through Pt clusters alloying with copper in zeolite. *Nano Res.* **2023**, *16*, 6537–6543. [[CrossRef](#)]
17. Liu, S.; Zhang, B.; Liu, G. Metal-based catalysts for the non-oxidative dehydrogenation of light alkanes to light olefins. *React. Chem. Eng.* **2021**, *6*, 9–26. [[CrossRef](#)]
18. Wang, G.-D.; Jiang, J.-W.; Sui, Z.-J.; Zhu, Y.-A.; Zhou, X.-G. Kinetic Promotion Effect of Hydrogen and Dimethyl Disulfide Addition on Propane Dehydrogenation over the Pt–Sn–K/Al₂O₃ Catalyst. *ACS Omega* **2022**, *7*, 30773–30781. [[CrossRef](#)]
19. Morgan, K.; Goguuet, A.; Hardacre, C. Metal Redispersion Strategies for Recycling of Supported Metal Catalysts: A Perspective. *ACS Catal.* **2015**, *5*, 3430–3445. [[CrossRef](#)]
20. Borgna, A.; Garetto, T.F.; Apesteguía, C.R.; Le Normand, F.; Moraweck, B. Sintering of Chlorinated Pt/γ-Al₂O₃ Catalysts: An In Situ Study by X-ray Absorption Spectroscopy. *J. Catal.* **1999**, *186*, 433–441. [[CrossRef](#)]
21. Borgna, A.; Le Normand, F.; Garetto, T.F.; Apesteguía, C.R.; Moraweck, B. X-ray Absorption Spectroscopy: A powerful tool to investigate intermediate species during sintering-redispersion of metallic catalysts. In *Studies in Surface Science and Catalysis*; Delmon, B., Froment, G.F., Eds.; Elsevier: Amsterdam, The Netherlands, 1999; Volume 126, pp. 179–186.
22. Hung, C.-C.; Yeh, C.-Y.; Shih, C.-C.; Chang, J.-R. Oxychlorination Redispersion of Pt Catalysts: Surface Species and Pt-Support Interactions Characterized by X-ray Absorption and FT-IR Spectroscopy. *Catalysts* **2019**, *9*, 362. [[CrossRef](#)]
23. Dai, Y.; Lu, P.; Cao, Z.; Campbell, C.T.; Xia, Y. The physical chemistry and materials science behind sinter-resistant catalysts. *Chem. Soc. Rev.* **2018**, *47*, 4314–4331. [[CrossRef](#)]
24. Monzón, A.; Garetto, T.F.; Borgna, A. Sintering and redispersion of Pt/γ-Al₂O₃ catalysts: A kinetic model. *Appl. Catal. A Gen.* **2003**, *248*, 279–289. [[CrossRef](#)]
25. Susu, A.A.; Ogogo, E.O.; Ngomo, H.M. The effect of sintering-redispersion on the selective aromatic yield on supported platinum catalysts. *Chem. Eng. Res. Des.* **2006**, *84*, 664–676. [[CrossRef](#)]
26. Gracia, F.J.; Miller, J.T.; Kropf, A.J.; Wolf, E.E. Kinetics, FTIR, and Controlled Atmosphere EXAFS Study of the Effect of Chlorine on Pt-Supported Catalysts during Oxidation Reactions. *J. Catal.* **2002**, *209*, 341–354. [[CrossRef](#)]
27. Anderson, J.A.; Fernandez-Garcia, M. Use of IR and XANES to monitor catalysts during preparation, regeneration and reaction. *Chem. Eng. Res. Des.* **2000**, *78*, 935–942. [[CrossRef](#)]
28. Arteaga, G.J.; Anderson, J.A.; Becker, S.M.; Rochester, C.H. Influence of oxychlorination treatment on the surface and bulk properties of a Pt–Sn/Al₂O₃ catalyst. *J. Mol. Catal. A Chem.* **1999**, *145*, 183–201. [[CrossRef](#)]
29. Le Normand, F.; Borgna, A.; Garetto, T.F.; Apesteguía, C.R.; Moraweck, B. Redispersion of Sintered Pt/Al₂O₃ Naphtha Reforming Catalysts: An in Situ Study Monitored by X-ray Absorption Spectroscopy. *J. Phys. Chem.* **1996**, *100*, 9068–9076. [[CrossRef](#)]
30. Rojek, J.; Nosewicz, S.; Maździarz, M.; Kowalczyk, P.; Wawrzyk, K.; Lumelskyj, D. Modeling of a Sintering Process at Various Scales. *Procedia Eng.* **2017**, *177*, 263–270. [[CrossRef](#)]
31. Li, Z.; Ji, S.; Liu, Y.; Cao, X.; Tian, S.; Chen, Y.; Niu, Z.; Li, Y. Well-Defined Materials for Heterogeneous Catalysis: From Nanoparticles to Isolated Single-Atom Sites. *Chem. Rev.* **2020**, *120*, 623–682. [[CrossRef](#)]
32. Thommes, M.; Kaneko, K.; Neimark, A.V.; Olivier, J.P.; Rodriguez-Reinoso, F.; Rouquerol, J.; Sing, K.S.W. Physisorption of gases, with special reference to the evaluation of surface area and pore size distribution (IUPAC Technical Report). *Pure Appl. Chem.* **2015**, *87*, 1051–1069. [[CrossRef](#)]
33. Wang, H.-Z.; Sun, L.-L.; Sui, Z.-J.; Zhu, Y.-A.; Ye, G.-H.; Chen, D.; Zhou, X.-G.; Yuan, W.-K. Coke Formation on Pt–Sn/Al₂O₃ Catalyst for Propane Dehydrogenation. *Ind. Eng. Chem. Res.* **2018**, *57*, 8647–8654. [[CrossRef](#)]
34. Kwak, J.H.; Hu, J.Z.; Mei, D.; Yi, C.W.; Kim, D.H.; Peden, C.H.F.; Allard, L.F.; Szanyi, J. Coordinatively Unsaturated Al³⁺ Centers as Binding Sites for Active Catalyst Phases of Platinum on gamma-Al₂O₃. *Science* **2009**, *325*, 1670–1673. [[CrossRef](#)]
35. Virnovskaia, A.; Morandi, S.; Rytter, E.; Ghiotti, G.; Olsbye, U. Characterization of Pt,Sn/Mg(Al)O catalysts for light alkane dehydrogenation by FT-IR Spectroscopy and catalytic measurements. *J. Phys. Chem. C* **2007**, *111*, 14732–14742. [[CrossRef](#)]
36. Arteaga, G.J.; Anderson, J.A.; Rochester, C.H. FTIR study of CO adsorption on coked Pt–Sn/Al₂O₃ catalysts. *Catal. Lett.* **1999**, *58*, 189–194. [[CrossRef](#)]
37. Kaylor, N.; Davis, R.J. Propane dehydrogenation over supported Pt–Sn nanoparticles. *J. Catal.* **2018**, *367*, 181–193. [[CrossRef](#)]
38. Pieck, C.L.; Jablonski, E.L.; Parera, J.M. Sintering-redispersion of Pt–Re/Al₂O₃ during regeneration. *Appl. Catal.* **1990**, *62*, 47–60. [[CrossRef](#)]
39. Serrano-Ruiz, J.C.; Huber, G.W.; Sánchez-Castillo, M.A.; Dumesic, J.A.; Rodríguez-Reinoso, F.; Sepúlveda-Escribano, A. Effect of Sn addition to Pt/CeO₂–Al₂O₃ and Pt/Al₂O₃ catalysts: An XPS, ¹¹⁹Sn Mössbauer and microcalorimetry study. *J. Catal.* **2006**, *241*, 378–388. [[CrossRef](#)]

40. Lieske, H.; Lietz, G.; Spindler, H.; Völter, J. Reactions of platinum in oxygen- and hydrogen-treated Pt γ -Al₂O₃ catalysts: I. Temperature-programmed reduction, adsorption, and redispersion of platinum. *J. Catal.* **1983**, *81*, 8–16. [[CrossRef](#)]
41. Zhang, W.; Wang, H.; Jiang, J.; Sui, Z.; Zhu, Y.; Chen, D.; Zhou, X. Size Dependence of Pt Catalysts for Propane Dehydrogenation: From Atomically Dispersed to Nanoparticles. *ACS Catal.* **2020**, *10*, 12932–12942. [[CrossRef](#)]
42. Sattler, A.; Paccagnini, M.; Liu, L.; Gomez, E.; Klutse, H.; Burton, A.W.; Corma, A. Assessment of metal-metal interactions and catalytic behavior in platinum-tin bimetallic subnanometric clusters by using reactive characterizations. *J. Catal.* **2021**, *404*, 393–399. [[CrossRef](#)]
43. Campbell, C.T. The Energetics of Supported Metal Nanoparticles: Relationships to Sintering Rates and Catalytic Activity. *Acc. Chem. Res.* **2013**, *46*, 1712–1719. [[CrossRef](#)]
44. Yang, M.L.; Zhu, Y.A.; Fan, C.; Sui, Z.J.; Chen, D.; Zhou, X.G. DFT study of propane dehydrogenation on Pt catalyst: Effects of step sites. *Phys. Chem. Chem. Phys.* **2011**, *13*, 3257–3267. [[CrossRef](#)] [[PubMed](#)]
45. Liu, Y.; Zong, X.; Patra, A.; Caratzoulas, S.; Vlachos, D.G. Propane Dehydrogenation on Pt_xSn_y (x, y ≤ 4) Clusters on Al₂O₃(110). *Acs Catal.* **2023**, *13*, 2802–2812. [[CrossRef](#)]
46. Zhou, X.; Zhang, Y.; Wang, J. DFT study on the regeneration of Pt/ γ -Al₂O₃ catalyst: The effect of chlorine on the redispersion of metal species. *Appl. Surf. Sci.* **2021**, *545*, 148988. [[CrossRef](#)]
47. Hu, S.; Li, W.-X. Sabatier principle of metal-support interaction for design of ultrastable metal nanocatalysts. *Science* **2021**, *374*, 1360–1365. [[CrossRef](#)]
48. Kamiuchi, N.; Taguchi, K.; Matsui, T.; Kikuchi, R.; Eguchi, K. Sintering and redispersion of platinum catalysts supported on tin oxide. *Appl. Catal. B Environ.* **2009**, *89*, 65–72. [[CrossRef](#)]
49. DeLaRiva, A.T.; Hansen, T.W.; Challa, S.R.; Datye, A.K. In situ Transmission Electron Microscopy of catalyst sintering. *J. Catal.* **2013**, *308*, 291–305. [[CrossRef](#)]
50. Zhu, X.; Wang, T.; Xu, Z.; Yue, Y.; Lin, M.; Zhu, H. Pt-Sn clusters anchored at Al-penta(3+) sites as a sinter-resistant and regenerable catalyst for propane dehydrogenation. *J. Energy Chem.* **2022**, *65*, 293–301. [[CrossRef](#)]
51. Zhang, W.; Ma, H.; Wang, H.; Jiang, J.; Sui, Z.; Zhu, Y.-A.; Chen, D.; Zhou, X. Tuning partially charged Pt δ^+ of atomically dispersed Pt catalysts toward superior propane dehydrogenation performance. *Catal. Sci. Technol.* **2021**, *11*, 7840–7843. [[CrossRef](#)]
52. Zeeshan, M.; Chang, Q.-Y.; Zhang, J.; Hu, P.; Sui, Z.-J.; Zhou, X.-G.; Chen, D.; Zhu, Y.-A. Effects of Oxygen Vacancy and Pt Doping on the Catalytic Performance of CeO₂ in Propane Dehydrogenation: A First-Principles Study. *Chin. J. Chem.* **2021**, *39*, 2391–2402. [[CrossRef](#)]
53. Zhang, R.; Chang, Q.-Y.; Ma, F.; Zeeshan, M.; Yang, M.-L.; Sui, Z.-J.; Chen, D.; Zhou, X.-G.; Zhu, Y.-A. Enhanced catalytic performance of transition metal-doped Cr₂O₃ catalysts for propane dehydrogenation: A microkinetic modeling study. *Chem. Eng. J.* **2022**, *446*, 136913. [[CrossRef](#)]
54. Fiedorow, R.M.J.; Wanke, S.E. The sintering of supported metal catalysts: I. Redispersion of supported platinum in oxygen. *J. Catal.* **1976**, *43*, 34–42. [[CrossRef](#)]
55. Straguzzi, G.I.; Aduriz, H.R.; Gigola, C.E. Redispersion of platinum on alumina support. *J. Catal.* **1980**, *66*, 171–183. [[CrossRef](#)]
56. Lee, T.J.; Kim, Y.G. Redispersion of supported platinum catalysts. *J. Catal.* **1984**, *90*, 279–291. [[CrossRef](#)]
57. Otto, K.; Weber, W.H.; Graham, G.W.; Shyu, J.Z. Identification of dispersed platinum on -alumina by laser-Raman spectroscopy. *Appl. Surf. Sci.* **1989**, *37*, 250–257. [[CrossRef](#)]

Disclaimer/Publisher's Note: The statements, opinions and data contained in all publications are solely those of the individual author(s) and contributor(s) and not of MDPI and/or the editor(s). MDPI and/or the editor(s) disclaim responsibility for any injury to people or property resulting from any ideas, methods, instructions or products referred to in the content.